Separation Science and Technology
Publication details, including instructions for authors and subscription information:
http://www.informaworld.com/smpp/title~content=t713708471

Desalination by Membrane Distillation: A Parametric Study

Fawzi A. Banat; Jana Simandl

To cite this Article Banat, Fawzi A. and Simandl, Jana(1998) 'Desalination by Membrane Distillation: A Parametric Study', Separation Science and Technology, 33: 2, 201 — 226
To link to this Article: DOI: 10.1080/01496399808544764
URL: http://dx.doi.org/10.1080/01496399808544764

SEPARATION SCIENCE AND TECHNOLOGY, 33(2), pp. 201–226, 1998

Desalination by Membrane Distillation: A Parametric Study

FAWZI A. BANAT*
DEPARTMENT OF CHEMICAL ENGINEERING
JORDAN UNIVERSITY OF SCIENCE AND TECHNOLOGY
PO BOX 3030, IRBID, JORDAN

JANA SIMANDL
DEPARTMENT OF CHEMICAL ENGINEERING
McGILL UNIVERSITY
3480 UNIVERSITY STREET, MONTREAL, QUEBEC, CANADA

ABSTRACT

Membrane distillation was investigated as a possible technique for desalination. An air-gap module with built-in condensing surface was used for conducting experiments on polyvinylidene fluoride flat membrane sheets. The feed stream tested was artificial seawater. The quality of the permeate, quantified by conductivity measurements, and the permeate flux were monitored as the feed temperature, feed flow rate, cooling temperature, and cooling water flow rate were varied. The effect of the distance between the membrane and condensing surface was investigated by adjusting the air gap within the module. A mathematical model incorporating temperature and concentration polarization effects was developed and validated on the experimental data. Good agreement between experimental and predicted values was obtained.

INTRODUCTION

The availability of potable water is a major problem in numerous regions of the world. Due to population growth, desertification, and pollution, the problem of water purity is expected to become more acute in the future.

* To whom correspondence should be addressed.

According to the World Health Organization, drinking water salinity should be less than 500 ppm (1). However, the maximum permissible concentration of salts in drinking water depends on the type of salt and the total daily water consumption. The daily amount of drinking water needed by humans varies between 2 and 8 liters per person (1).

Desalination processes can broadly be divided into two categories:

1. Processes with a phase change, e.g., evaporation and distillation
2. Processes without a phase change, e.g., membrane reverse osmosis and electrdialysis

Distillation and evaporation methods for saline water desalination are based on the fact that water is volatile but the salts are not. Although the efficiency of the process can be improved by using configurations with multiple effects and multistage flash, the high energy requirements of this approach limit its large-scale application to areas where affordable fuel is available.

Membrane distillation (MD), the method investigated in this work, is a hybrid of thermal distillation and membrane processes in which a microporous hydrophobic membrane separates a warm solution from a cooler chamber which contains either a liquid or a gas. As the process is nonisothermal, vapor molecules migrate through the membrane pores from the high to the low vapor pressure side, that is, from the warmer to the cooler compartment. It is also possible to lower the vapor pressure isothermally by using concentrated solutions or applying vacuum in the downstream side. The separation mechanism of membrane distillation is based on vapor–liquid equilibrium. The transport mechanism of membrane distillation involves four steps:

1. Movement of the volatile components from the bulk of the feed stream to the membrane surface
2. Evaporation of the volatiles in the warm feed at the membrane surface
3. Migration of the vapor through the nonwetted pores
4. Condensation of the vapor at the cold permeate side either in a liquid or in a condenser

Among membrane distillation processes, variations exist as to the method by which the vapor is recovered once it has migrated through the membrane. These alternatives are:

1. Direct contact membrane distillation (DCMD), the oldest and most widely used process, has liquid phases in direct contact with both sides of the membrane. The vapor diffusion path is limited to the thickness of the membrane, thereby reducing mass and heat transfer resistances.

Condensation within the pores is avoided by selecting appropriate temperature differences across the membrane.

2. Air-gap membrane distillation (AGMD) has an additional air gap interposed between the membrane and the condensation surface. This gives rise to higher heat and mass transfer resistances. Although heat loss by conduction is reduced, the penalty is flux reduction. The use of an air-gap configuration allows larger temperature differences to be applied across the membrane, which can compensate in part for the greater transfer resistances.

The possible applications of membrane distillation are limited by the wettability of the membrane, which is a function of the feed surface tension. Therefore, aqueous solutions containing inorganic solutes or low concentrations of volatile organic compounds can be treated while solutions with surface-active components cannot. The other major consideration in membrane selection for this process is pore size and porosity. High porosities are of special interest since the area available for evaporation is directly related to flux. However, high porosities are usually associated with large pore sizes which are undesirable because they increase the risk of membrane wetting. Membranes with 60 to 80% porosity and 0.1–0.5 μm pore size offer a suitable compromise. Hydrophobic microporous membranes such as those made from polypropylene (PP), polytetrafluoroethylene (PTFE), polyethylene (PE), and polyvinylidene fluoride (PVDF) can meet these requirements (2). Applying a thin hydrophobic coat upon a cheaper substrate is also a viable alternative (3). Commercially, membranes suitable for membrane distillation are available in flat sheet, hollow fiber, and tubular forms. These membranes are not marketed for membrane distillation but rather as specialized microfiltration membranes.

In membrane distillation the desired product can be either the permeate or the concentrate solution. Tests of MD for the following applications have been reported in the literature: production of pure water from brackish water or seawater (4, 5); concentration of mandarin orange juice (6), grape juice (7), milk, sugar, and gelatin solutions (8); blood concentration (9); and extraction of dilute ethanol from aqueous solutions (10) or from fermentation broths (11).

The main advantages of membrane distillation over conventional distillation processes are: lower operating temperatures, compact modules, mist elimination, and the possibility of overcoming corrosion problems by using plastic equipment. This process can use such available energy sources as solar energy or waste energy in industrial processes. However, process still suffers from the dangers of membrane wetting and high membrane cost. Development of new highly hydrophobic membranes with an

appropriate pore size, new membrane coatings, and increased competition among manufacturers should reduce the latter drawback (2).

When MD is used for desalination, salt water is the hot feed solution. Pure water vapor passes through the membrane pores while the salts and other nonvolatiles remain on the warm side of the membrane. The possible application of membrane distillation for desalination has been examined by some researchers (12–14). The studies reported in the literature were preliminary and on a laboratory scale. Although two commercial units operated briefly in the Cayman Islands and Florida Keys (15), no information has been published about these operations.

In this study, an air-gap module with an adjustable air gap was used to study the fundamental characteristics of air-gap membrane distillation. The feed solution was an artificially prepared seawater that was identical to natural seawater but free of biological life. A fully predictive mathematical model, based on the first principles of heat and mass transfer and incorporating the temperature and concentration polarization effects, was developed and validated with the experimental data.

EXPERIMENTAL

The concept of crossflow cells was adjusted to suit the membrane distillation process. An air gap of adjustable width was introduced. The membrane sheets were readily removable for replacement or treatment. The unit was constructed of Plexiglas to permit monitoring of the flow pattern in the cell.

The cell length and width were 21.5 and 16.5 cm, respectively, with a Plexiglas thickness of 3 cm. It had an adjustable air gap which separated the cell into two compartments: the feed compartment where the warm solution directly contacts the membrane and the cooling compartment where a cooling liquid passes on one side of the condensation plate. To ensure that the feed had easy access to the entire membrane surface, distribution holes of 1 mm diameter were located at the inlet channels of both compartments. Observation through the Plexiglas confirmed that this distribution system was effective. The exposed membrane area was 160 cm^2.

The air-gap thickness was adjusted by using multiple layers of white neoprene rubber (Albion 920). The thickness of each gasket was $\frac{1}{16}$ inch. To avoid membrane bending, wrinkling, and pocketing, a stainless steel perforated plate was used as a membrane support. The permeate vapor diffused through the membrane pores, and the air gap was collected on the cooling plate. High thermal conductivity requirements and resistance

to corrosion led to the use of stainless steel as a condensing surface. An inclined circular channel was drilled at the cell bottom through the cooling compartment and the condensing plate to collect the condensed vapors. The channel diameter was 1.3 cm. The collected permeate was measured by its meniscus rise in a graduated cylinder.

The overall membrane distillation system is shown in Fig. 1. The temperature of the hot feed was kept constant by using a proportional control-

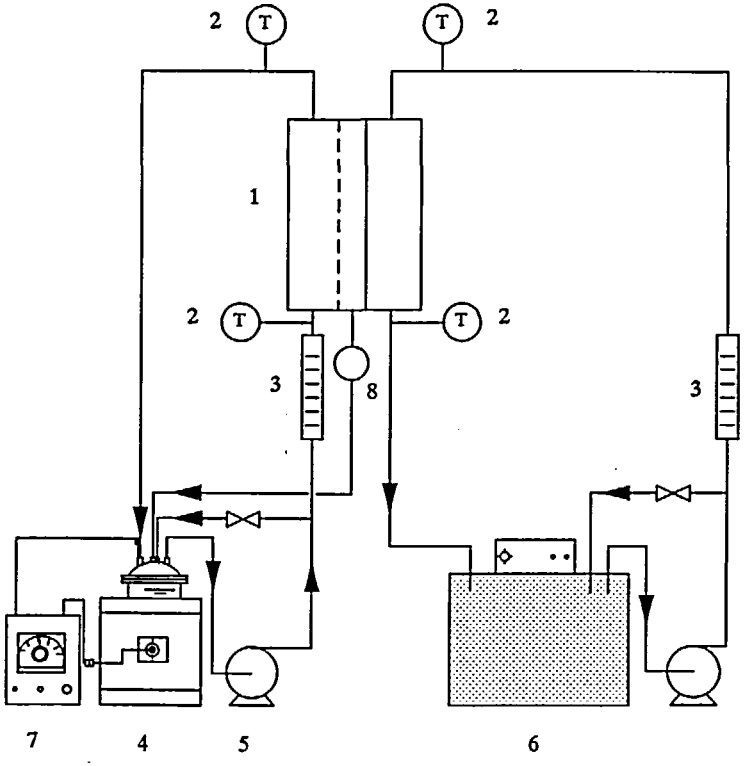

1. Membrane cell
2. Thermocouple
3. Rotameter
4. Feed solution
5. Centrifugal pump
6. Cooling water
7. Proportional controller
8. Permeate measurement and collection

FIG. 1 Schematic drawing of the air-gap membrane distillation process.

ler connected to a heating mantel. The cooling liquid temperature was kept constant by using a Neslab RTE-220 cooling bath. Two magnetic chemical resistant centrifugal pumps (Baldor, TE-5C-MD) were used to circulate the liquid between the feeding vessels and the cell. Rotameters (Brooks, model 1358EZ59) with a capacity up to 5.7 L/min were used to measure the feed flow rates. The inlet and outlet temperatures from the cell were monitored using copper–constantan type T thermocouples.

Durapore flat sheet membranes, manufactured by Millipore Co., were used in these experiments. Durapore membranes are polyvinylidene fluoride (PVDF) of 0.45 μm pore diameter, 0.11 mm membrane thickness, and 75% porosity (manufacturer specifications).

Simulated seawater was prepared by dissolving salt crystals produced by Marine Enterprises Inc. to a specific gravity of 1.020 to 1.022. A partial list of the constituents is given in Table 1 (16). According to the manufacturer, this solution is within the range of seawater compositions.

THEORY

In order to deepen understanding of the membrane distillation process and to analyze the experimental results obtained for the desalination, a fully predictive mathematical model was developed. Based on first principles, it does not include any tuning parameters but does require estimates of such membrane properties as tortuosity and void fraction. The model equations incorporate the steps involved in transferring the more volatile components from the bulk feed solution into the permeate stream and associated phenomena.

TABLE 1
Partial List of Species Present in Reconstituted Seawater Used in Experiments (16)

Element	Concentration (ppm)
Cl	18,600
Na	10,400
Mg	1,290
Ca	410
K	380
Br	62
B	4.9
F	1.9

Vapor migration from the feed side to the cooling surface results from a vapor-pressure gradient caused by a temperature difference across the unit. The mass transfer steps involve movement within the liquid feed toward the membrane surface, evaporation at the membrane interface, and transport of the vapor through the membrane pores and air gap prior to condensation.

Two phenomena which play an important role in membrane distillation are concentration and temperature polarization. When a molecular mixture is brought to the membrane surface by the driving force action, some molecules will permeate through the membrane while others will be retained. This leads to an accumulation of the retained components and a depletion of the more permeating components in the boundary layer adjacent to the membrane surface. This phenomenon is referred to as concentration polarization. Since membrane distillation involves simultaneous heat and mass transfer, the heat required for species evaporation at the membrane–liquid interface has to be supplied from the bulk solution. This creates temperature gradients in the liquid film adjoining the membrane. This phenomenon is called temperature polarization.

As the process in membrane distillation is nonisothermal, the composition and flux of the permeating species can be determined based on the relationship between:

- Molar flux and concentration gradient
- Energy flux and temperature gradient
- Vapor–liquid equilibrium (VLE)

Mass transfer in membrane distillation is accompanied by heat transfer along the path of migration. In this case the temperature and concentration gradients will be established in the diffusional films as shown in Fig. 2.

Mass Transfer

The molar vapor diffusion flux of water through a stagnant gas film (C) is known as Stefan diffusion and is given by

$$N_w = -\frac{cD_{wc}}{1 - y_w}\frac{dy_w}{dz} \tag{1}$$

where y_w is the mole fraction of water vapor and c is its molar density. According to the ideal gas law:

$$c = P/RT \tag{2}$$

where P is the total pressure, R is the ideal gas constant, and T is the average temperature. The diffusion coefficient can be related to tempera-

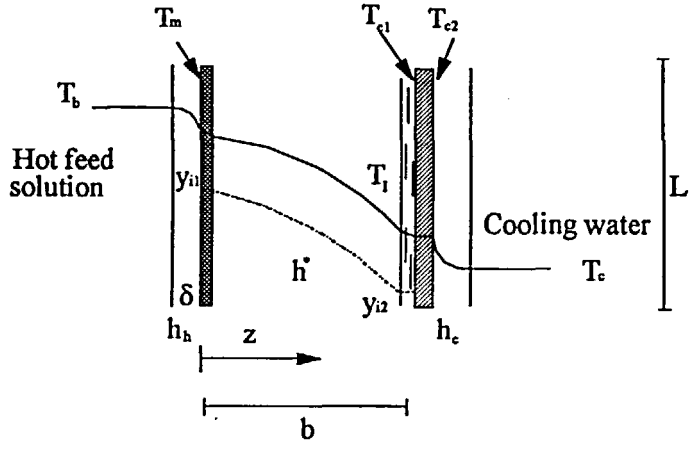

FIG. 2 Temperature profile in an air-gap membrane distillation module.

ture by (17)

$$D_T = D_0 \left[\frac{T}{T_0}\right]^{1.75} \tag{3}$$

A differential mass balance over a control volume for steady-state operations yields

$$dN_w/dz = 0 \tag{4}$$

This relation stipulates a constant molar flux of water throughout the gas phase from the membrane interface to the cooling surface. Equation (1), combined with Eq. (2), can be integrated with the following boundary conditions:

$$z = 0, \quad y_i = y_{w1} \tag{5}$$

$$z = b, \quad y_i = y_{w2}$$

The molar flux in terms of pressure will then be

$$N_w = \frac{D_{wC}P}{RTbp^*_{C,lm}}(p^*_{w1} - p^*_{w2}) \tag{6}$$

where b is the air gap thickness, p^*_w is the partial pressure of water and $p^*_{C,lm}$ is the log mean partial pressure difference of the stagnant component

defined as

$$p_{C,lm} = \frac{p_{C2} - p_{C1}}{\ln \frac{p_{C2}}{p_{C1}}} \tag{7}$$

To account for the membrane porosity (ϵ), thickness (δ), and tortuosity (τ), the effective molar flux becomes

$$N_w = \frac{\epsilon D_{wC} P}{RTp^*_{C,lm}} \left[\frac{1}{\delta\tau + b}\right] (p^*_{w1} - p^*_{w2}) \tag{8}$$

Heat Transfer

For the calculations of the permeate composition by means of the vapor–liquid equilibrium equations, it is essential that the interfacial temperatures of the feed and the condensation surface be known at the membrane and condensation surface interfaces. These temperatures cannot be measured experimentally but can be estimated by energy flux calculations.

For processes which involve simultaneous heat and mass transfer as in membrane distillation, there is heat flux that occurs as a result of the interdiffusion of species, and conductive heat flux due to temperature differences. The stages of heat transfer in membrane distillation include heat flux from the feed bulk to the membrane surface, from the membrane surface to the condensation interface, and from the condensate interface to the coolant bulk temperature.

Heat Flux from the Feed Bulk to the Membrane Surface

Heat flux from the feed bulk to the membrane surface can be written as

$$q = h_{hf}(T_b - T_m) + N_w Cp_{lw}(T_b - T_m) = h_h(T_b - T_m) \tag{9}$$

$$h_h = (h_{hf} + N_w Cp_{lw}) \tag{10}$$

where h_{hf} is the liquid film heat transfer coefficient, and Cp_{lw} is the liquid-phase specific heat.

From the Membrane to the Condensate Surface

The total flux through the air gap is made up of two parts: one is the sensible heat flux q_s and the other is due to vaporization at the hot membrane surface.

$$q = q_s + N_w \lambda_w \tag{11}$$

The sensible heat flux in general contains the following contributions (18):

1. Sensible heat carried by conduction in the normal manner without mass transfer
2. Sensible heat carried bodily by the transferring substances

Hence:

$$q_s = -k\frac{dT}{dz} + N_w Cp_g(T - T_1) \tag{12}$$

where Cp_g is the specific heat of the gas and k is the gas-phase thermal conductivity. In proceeding to obtain the temperature profile and heat flux, it is convenient to define the following parameters.

(i) A dimensionless distance within the film:

$$\eta = z/b \tag{13}$$

where b is the thickness of the air gap and z is the distance from the membrane interface in contact with the feed solution.

(ii) A "zero flux" heat transfer coefficient in the gaseous phase:

$$h_y = k/b \tag{14}$$

(iii) A dimensionless heat transfer rate factor:

$$\theta = N_w Cp_g/h_y \tag{15}$$

where θ is in the form of Peclet number which is the ratio of heat transfer by convection to conduction.

Substituting Eqs. (13)–(15) into Eq. (12) yields

$$q_s = -h_y\frac{dT}{d\eta} + h_y\theta(T - T_1) \tag{16}$$

From the energy balance around a differential element in the air gap,

$$dq_s/dz = 0 \tag{17}$$

by substituting Eq. (16) into Eq. (17):

$$-h_y\frac{d^2T}{d\eta^2} + h_y\theta\frac{dT}{d\eta} = 0 \tag{18}$$

Equation (18) may be integrated for the following boundary conditions:

$$\eta = 0, \quad T = T_m$$

$$\eta = 1, \quad T = T_1$$

to give the following temperature profile

$$\frac{T - T_m}{T_I - T_m} = \frac{1 - e^{\theta\eta}}{1 - e^{\theta}} \tag{19}$$

The conductive heat flux q_0 may be obtained by differentiating equation 19 to give

$$q_0 = -h_y \left.\frac{dT}{d\eta}\right|_{\eta=0} = h_y \frac{\theta}{e^{\theta} - 1}(T_m - T_I) \tag{20}$$

The factor $\theta/(e^{\theta} - 1)$ gives the effect of finite mass transfer rates on the heat transfer coefficient h_y. The sensible heat flux q_s is obtained by integrating Eq. (18) with the boundary conditions, or by adding Eq. (20) to the second right-hand part of Eq. (12) to give

$$q_s = h_y \frac{\theta e^{\theta}}{e^{\theta} - 1}(T_m - T_I) \tag{21}$$

$$= h_y \frac{\theta}{1 - e^{-\theta}}(T_m - T_I) \tag{22}$$

The Akerman correction factor $\theta/(1 - e^{-\theta})$ appearing in Eq. (22) accounts for the sensible heat transferred by diffusing vapors. In the absence of condensation, this factor equals 1 and increases as the rate of evaporation increases. The influence of mass transfer on the heat transfer process is included by combining h_y with the Ackerman factor (19):

$$h_y \frac{\theta}{1 - e^{-\theta}} = h_y + \left(\frac{1}{1 - e^{-\theta}} - \frac{1}{\theta}\right) N_w C p_g \tag{23}$$

Substituting Eq. (22) into Eq. (11) yields

$$q = h^*(T_m - T_I) + N_w \lambda_w \tag{24}$$

where

$$h^* = h_y \left(\frac{\theta}{1 - e^{-\theta}}\right)$$

From the Condensation Layer Interface to the Cold Bulk Liquid

$$q = h_d(T_I - T_{c1}) = \frac{k_c}{l}(T_{c1} - T_{c2}) \tag{25}$$

$$= h_{cf}(T_{c2} - T_c)$$

then

$$q = h_c(T_I - T_c) \tag{26}$$

$$h_c = \frac{1}{\frac{1}{h_d} + \frac{l}{k_c} + \frac{1}{h_{cf}}} \tag{27}$$

where h_d is the condensation heat transfer coefficient. k_c and l are the thermal conductivity and the thickness of the cooling plate, respectively.

Equations (9), (24), and (26) can be solved for the interfacial temperatures to give

$$T_m = T_b - \frac{U_T}{h_h}\left((T_b - T_c) + \frac{N_w\lambda_w}{h^*}\right) \tag{28}$$

$$T_I = T_c + \frac{U_T}{h_c}\left((T_b - T_c) + \frac{N_w\lambda_w}{h^*}\right) \tag{29}$$

where

$$U_T = \frac{1}{\frac{1}{h_h} + \frac{1}{h^*} + \frac{1}{h_c}} \tag{30}$$

and

$$q = U_T\left[(T_b - T_c) + \frac{N_w\lambda_w}{h^*}\right] \tag{31}$$

The value of the heat transfer coefficients can be calculated from the hydrodynamic conditions as follows. For laminar flow through ducts (20):

$$\mathrm{Nu} = 1.86(\mathrm{RePr})^{1/3}\left(\frac{dh}{L}\right)^{1/3}\left(\frac{\mu}{\mu_m}\right) \tag{32}$$

where μ is the fluid viscosity evaluated at the bulk temperature, μ_m is the fluid viscosity evaluated at the membrane interface temperature, d_h is the hydraulic diameter, and L is the duct length.

For fully developed turbulent flow

$$\mathrm{Nu} = 0.023\mathrm{Re}^{0.8}\mathrm{Pr}^n \tag{33}$$

The exponent n equals 0.4 for heating and 0.3 for cooling.

The value of the film condensation coefficient for vertical surfaces, h_d (21), is

$$h_d = 0.943 \left[\frac{\rho_l^2 g \lambda k_l^3}{\mu_l L \Delta T}\right]^{1/4} \tag{34}$$

where ρ_l and k_l are the fluid density and thermal conductivity at the film temperature, respectively, and g is the gravitational acceleration.

Concentration Polarization

The description of concentration polarization in membrane distillation is based on solute behavior. In desalination the salts are retained by the membrane and accumulate at the membrane surface. Therefore, their concentration will gradually increase. Such a concentration build up will generate a diffusive flow back to the bulk of the feed. When steady-state conditions are established, the convective solute flow to the membrane surface will be balanced by the solute flux through the membrane plus the diffusive flow from the membrane surface back to the bulk. Mathematically, this phenomenon can be described (22) as

$$\frac{c_m - c_p}{c_b - c_p} = \exp\left(\frac{J_v}{\kappa}\right) \tag{35}$$

where J_v is the volumetric flux ($m^3/m^2 \cdot s$) and κ is the liquid layer mass transfer coefficient $\kappa = D/\delta$ in which D is the molecular diffusivity and δ is the thickness of the boundary layer. The mass transfer coefficient for the diffusive mass transfer through the boundary layer can be obtained from Sherwood correlations (23).

For laminar flow through circular pipes:

$$\mathrm{Sh} = 1.86 \left(\mathrm{ReSc}\,\frac{d_h}{L}\right)^{1/3} \tag{36}$$

For turbulent flow through circular pipes:

$$\mathrm{Sh} = 0.023 \mathrm{Re}^{0.8} \mathrm{Sc}^{1/3} \tag{37}$$

Vapor–Liquid Equilibrium

If equilibrium is assumed to prevail at the interfaces, then the corresponding partial pressure is

$$p^* = (1 - x)p^\circ \tag{38}$$

where x is the mole fraction of the salt and p° is the vapor pressure of

water which is given by Antoine's equation (24)

$$\log p_i^\circ = A_i - \frac{B_i}{C_i + T} \tag{39}$$

where p° is in mmHg and T is in °C.

The presented equations were used in a computer program for water flux calculations.

RESULTS AND DISCUSSION

Experimental Reproducibility

The reproducibility of membrane distillation experiments was established by conducting the same set of feed temperature tests using six different membranes from the same commercial batch. Artificial seawater was used as a feed. As can be seen in Fig. 3, although the same trends were observed in all cases, some differences in absolute permeate flux values exist. The differences were more visible at the higher flux rates

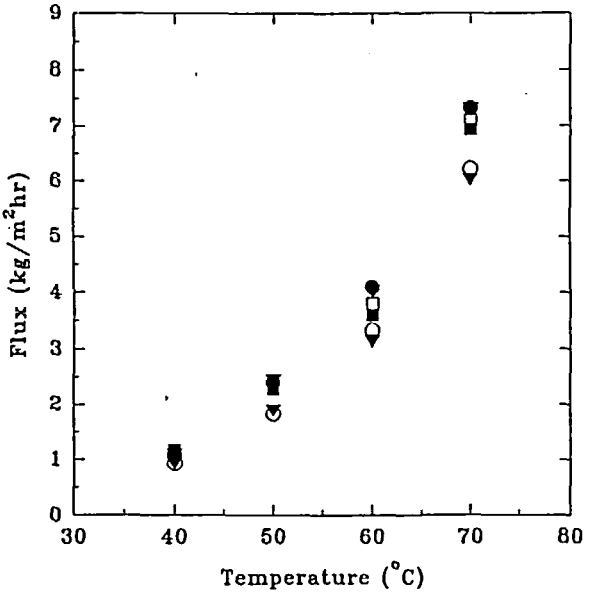

FIG. 3 Reproducibility of fluxes at different feed temperatures (T_c = 20°C, Q = 5.5 L/min, z = 0.35 cm).

resulting from high temperatures. From these tests the reproducibility of the permeate flux in membrane experiments is estimated to be ±20%. In all cases the conductivity of the permeate was 4 ± 1 μS/cm (less than 5 ppm salts).

Experimental and Predicted Effect of Operating Variables

Hot-Side Flow Rate

The effect of hot-side flow rate on flux is presented in Fig. 4. An increase in flow rate was accompanied by a slight increase in flux. This is because an increase in the hot-side flow rate increases the heat transfer coefficient in the boundary layer on the membrane surface, thereby reducing the temperature polarization effect. As the heat transfer coefficient increases, the surface temperature of the membrane on the hot-side approaches the feed stream bulk temperature. The model predicts different responses in the laminar and turbulent flow regions. Within the laminar region, the mass flux is expected to increase prior to approaching an asymptote. Here,

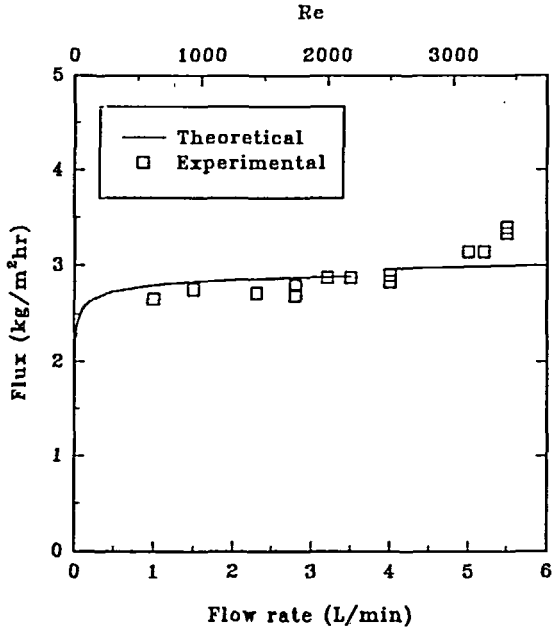

FIG. 4 Effect of hot-side flow rate on flux (T_h = 60°C, T_c = 20°C, z = 0.35 cm).

the agreement between experimental values and the model is very good. At the highest flow rates tested, the hydraulic pressure affected the membrane and increased the flux above expected values.

No effect of hot-side flow rate on permeate quality was observed. In all cases the conductivity was 4 ± 1 μS/cm. Overall, the value of operating at Reynolds numbers greater than 500 is dubious since only a small change in flux accompanies the increase in pumping cost.

Cold-Side Flow Rate Experiments

The nearly negligible effect of cold-side flow rate on the permeate flux is shown in Fig. 5. This result can be explained by studying the overall heat transfer coefficient which includes the hot-side, the air-gap, and the cold-side heat transfer coefficients. As the heat transfer coefficient in the air-gap is much smaller than the hot and the cold-side heat transfer coefficients, it will dominate the overall heat transfer coefficient. Hence, small changes in the cold-side flow rate will have little effect.

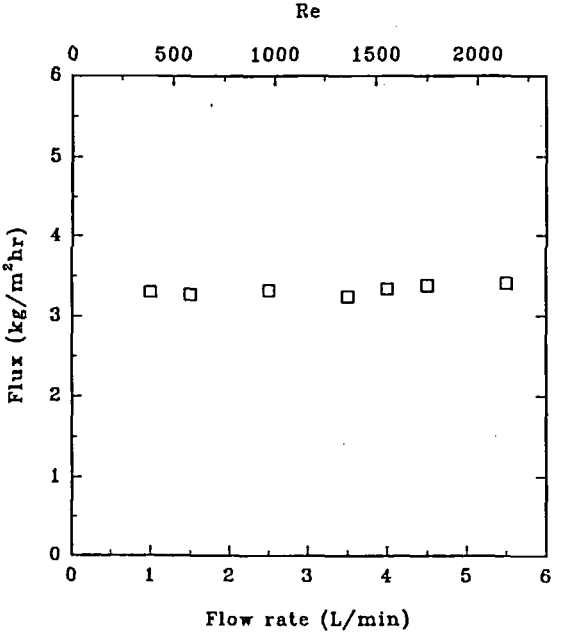

FIG. 5 Effect of cold-side flow rate on flux (T_h = 60°C, T_c = 20°C, Q_h = 5.5 L/min, z = 0.35 cm).

It should be pointed out that the significance of the heat transfer coefficient on the hot and the cold side is dependent on membrane module geometry and the fluid flow characteristics.

Long-Run Experiments

Figure 6 presents the results of a 10-day experiment conducted to examine the variation of flux over time. Initially, the flux increased until it reached a steady state. The transient time for the system to equilibrate was approximately 25 hours. At steady state the flux varied between 1.5 and 1.6 kg/m^2·h. The measured conductivity of the permeate was between 3 and 5 μS/cm.

Cold-Side Temperature

Figure 7 shows the effect of cold-side temperature on flux at a fixed hot-side temperature. The cold temperature was varied between 7 and 30°C. As shown, there is a gradual decrease in flux as the cold temperature rises. This negligible effect can be attributed to the low water vapor pres-

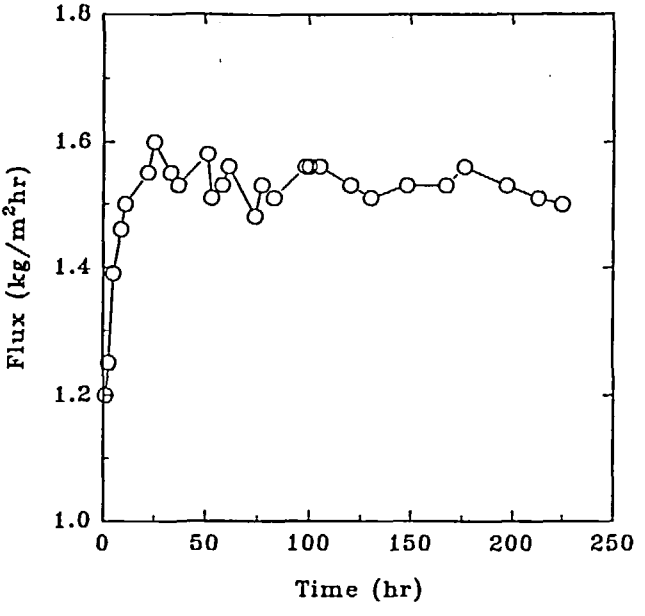

FIG. 6 Variation of flux vs time (T_h = 53°C, T_c = 7°C, z = 0.99 cm).

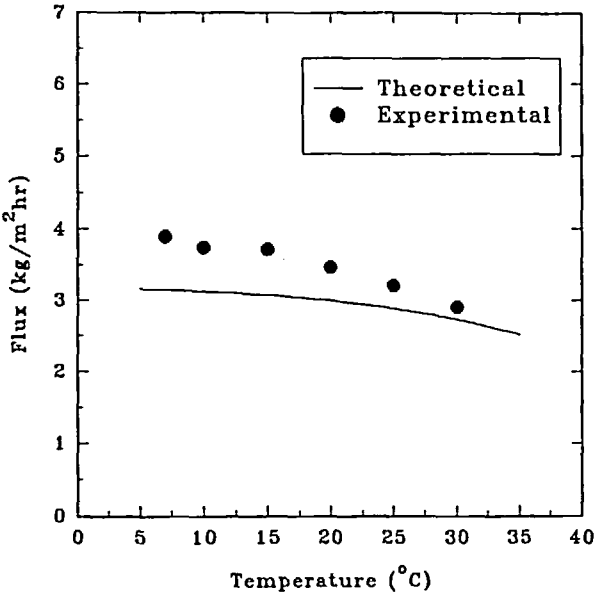

FIG. 7 Flux vs cold side temperature (T_h = 60°C, Q_h = 5.5 L/min, z = 0.35 cm).

sure sensitivity at lower temperatures. For example, the vapor pressure of water at 7°C is 7.53 mmHg while at 30°C it is 31.8 mmHg. Therefore, the vapor pressure difference will drop from 142 mmHg at 7°C to 118 mmHg at 30°C. Little benefit would be derived from cooling the cooling water since permeate flux is not very sensitive to this parameter.

The agreement between the model and the corresponding experimental points is better at high temperatures than at low ones. It is suspected that the steeper gradient between the hot and cold side creates density gradients. Any increase in natural convection due to this would not be accounted for within the model.

Hot-Side (feed stream) Temperature

Model predictions and experimental data are presented in Fig. 8 for the effect of hot-side temperature on permeate flux. An increase in temperature raised the flux rate exponentially. This can be explained by the Antoine equation (Eq. 39) which shows the exponential relation between the driving force (vapor pressure difference) and the temperature. In Fig. 9 the data are replotted, taking into account the relationship between vapor

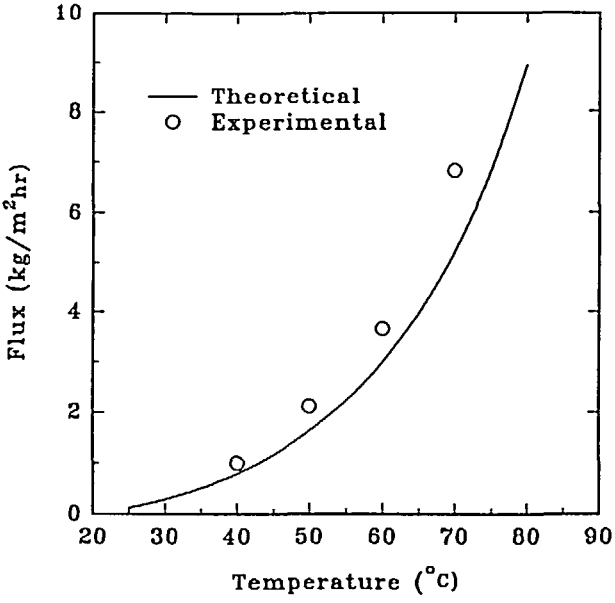

FIG. 8 Flux vs feed temperature (T_c = 20°C, Q_h = 5.5 L/min, z = 0.35 cm).

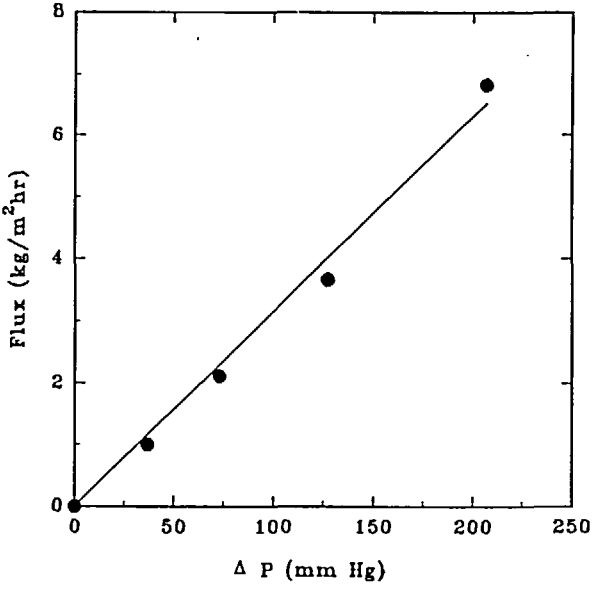

FIG. 9 Flux vs vapor pressure difference (T_c = 20°C, Q_h = 5.5 L/min, z = 0.35 cm).

pressure and temperature. A linear relationship is obtained. This suggests that the relationship between the flux and the pressure difference can be described by the relation

$$n = \beta \Delta P \tag{40}$$

where β is the membrane characteristic coefficient. A similar phenomenon was noticed by Drioli et al. (25). In light of the mass transfer theory in membrane distillation, the magnitude of β is expected to be a function of the physical nature of the permeating species, the turbulence conditions of the feed flow, the operating pressure of the feed side of the membrane, the membrane structure properties, and the module configuration.

The agreement between the model and the corresponding experimental points is better at low temperatures than at high ones. Increasing the hot-side temperature while keeping the cold-side temperature constant results in a steeper temperature gradient inside the air-gap. As was seen when steeper temperature gradients were produced by lowering the cooling water temperature, the density gradients may increase the natural convection contribution.

Air-Gap Width

The air-gap compartment in the module was designed and built to allow width variations via the insertion or removal of gaskets. In this way it was possible to vary the length of the path over which the vapor passes prior to condensation. In Fig. 10 the flux is presented for experiments in which all operating variables except the air-gap width were held constant. Figure 11 shows a comparison between theoretical predictions and experimental data for the effect of air-gap width. Differences between the two are attributed to the compartment geometry and its effect on fluid circulation. When the geometric ratio (ratio between vertical and horizontal dimension of the enclosure) approaches 1, the convective heat transfer effect reaches a maximum. Conversely, the convective heat transfer contribution vanishes ($Nu \rightarrow 1$) when the geometric ratio approaches zero or infinity (26). Keeping the enclosure height constant and varying the gap width will change the geometric ratio, thereby the mechanism of heat transfer may be shifted from pure conduction and diffusion to natural convection. The degree of natural convection occurring depends upon the geometric ratio.

In Fig. 12 the impact of air-gap width upon a series of hot-side temperatures is presented. As was expected, reducing the air-gap width increased the temperature gradient within the vapor compartment and increased flux. Both figures indicate that operating at small gap widths will maximize the flux. Kimura and Nakao (27) found the same effect of gap width on flux rate.

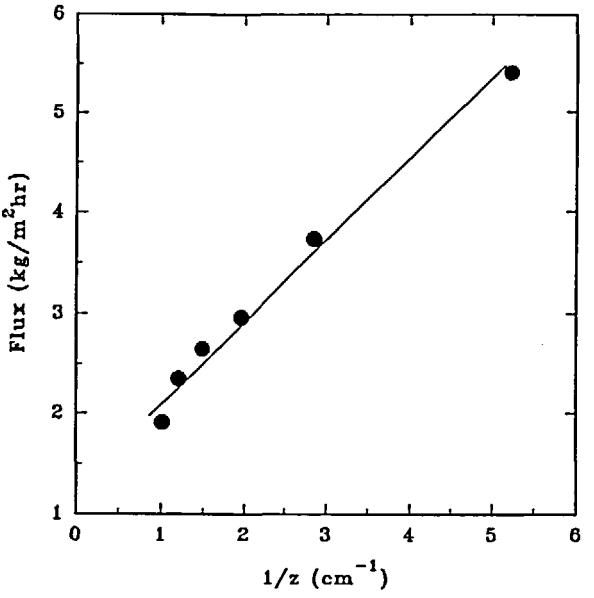

FIG. 10 Flux vs gap width inverse (T_h = 60°C, T_c = 20°C, Q_h = 5.5 L/min).

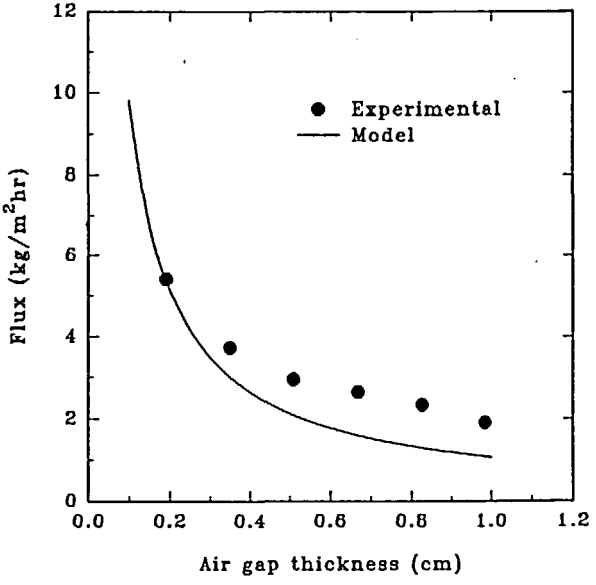

FIG. 11 Comparison of experimental and theoretical fluxes at different air gaps (T_h = 60°C, T_c = 20°C, Q_h = 5.5 L/min).

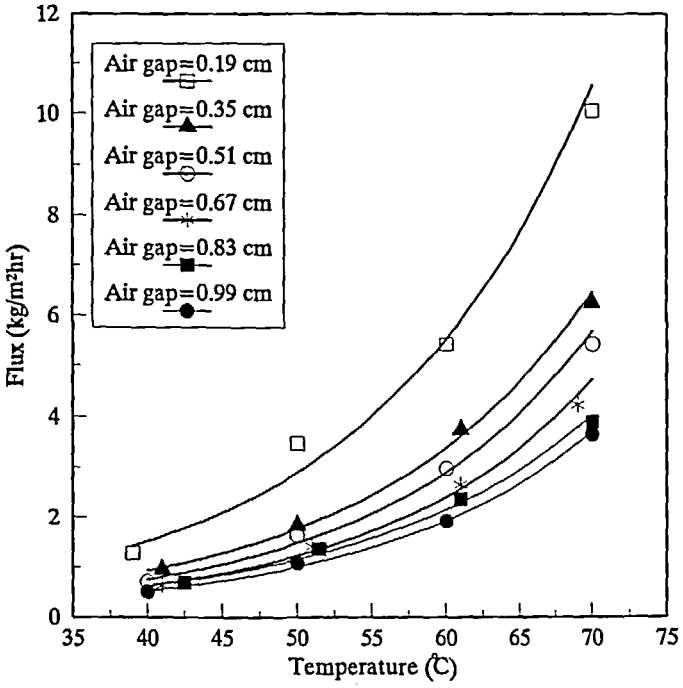

FIG. 12 Effect of air-gap thickness on flux at various feed temperatures (T_c = 20°C).

Evaporation Efficiency

Optimization of the membrane distillation process involves maximizing the permeate flux while minimizing the heat losses within the unit. It is not possible to perform a complete optimization without attaching some financial value to the permeate product and the heat used. Such financial values will vary with the site selected and the type of energy source used. In the absence of such values it is possible to examine the conflicting process effects by assessing an evaporation efficiency.

Membrane distillation is a combined heat and mass transfer process where the heat requirements represent a significant part of the process cost. The required heat contributes to: 1) the phase change from liquid to vapor of the permeate, 2) internal losses between the hot and cold streams, and 3) heat losses to the surroundings. Internal heat loss could be reduced by improvements in module design. For example, research

has been carried out to reduce heat loss in membrane modules without an air gap by deaeration (27) or by using thicker membranes (28). The introduction of an air gap reduces the heat loss by conduction across the membrane since the air acts as an insulating layer but it also reduces the mass transfer. Therefore, the internal evaporation efficiency (EE) can be defined as

$$\mathrm{EE} = n\lambda/q \tag{41}$$

where $n\lambda$ represents the heat which contributes to evaporation and q is the total heat transferred across the membrane. The heat lost (HL) through conduction for each kilogram of the produced flux can be calculated as

$$\mathrm{HL} = (q - n\lambda)/n \tag{42}$$

Based on these definitions, Fig. 13 shows the effect of the hot-side temperature on heat efficiency and heat loss. It is clear that operating at high temperatures increases the evaporation efficiency. This is mainly

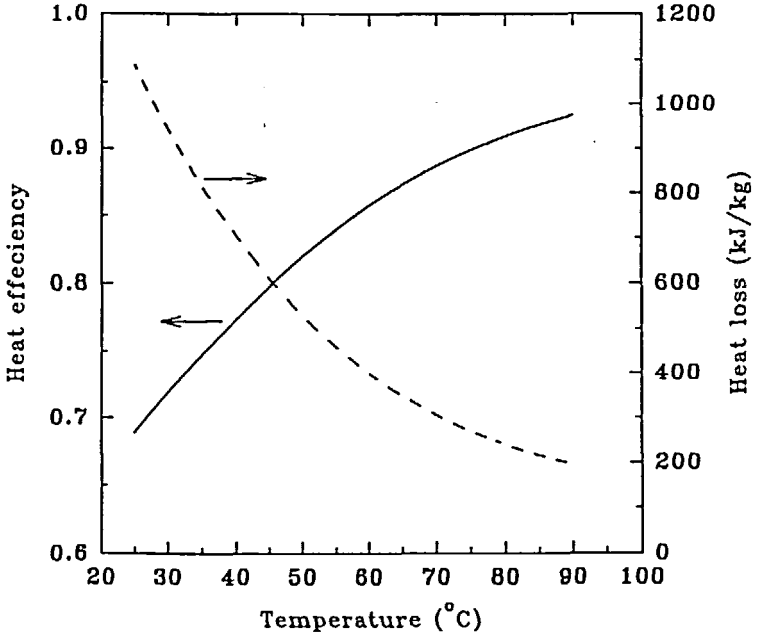

FIG. 13 Heat efficiency and loss vs feed temperature (T_c = 20°C, z = 0.35 cm, Re = 4000).

attributed to the exponentially increased mass flux with temperature rise. At high temperatures the amount of heat lost by conduction will be negligible in comparison with the heat transferred by the diffusing species. Therefore, from the heat transfer perspective it is better to operate at high temperatures than to operate at low ones.

CONCLUSIONS

The potential application of the membrane distillation process for desalination was experimentally assessed by conducting experiments on an adjustable air-gap module using PVDF flat-sheet membranes. Simulated seawater was used as a feed solution during the experiments. Very pure water with less than 5 ppm total solid content was obtained in all experiments. A fully predictive mathematical model incorporating the effects of temperature and concentration polarization was developed and validated with the experimental results. Based on the mathematical model developed and the experiments conducted, the following conclusions are drawn:

1. Time is required for the membrane to reach steady state.
2. The reproducibility of tests conducted with different membrane segments was ±20%.
3. Increasing the vapor pressure driving force increases the permeate flux. Given the exponential relationship between vapor pressure and temperature, this can best be achieved by increasing the feed temperature. Changes in the coolant temperature and flow rate have smaller effects.
4. Increasing the gap width increases the mass transfer resistance and inversely affects the flux.
5. The relation between flux and vapor pressure difference can be approximated by the linear form $N = \beta \Delta P$.
6. Operating at high temperatures is better than operating at low ones.
7. The mathematical model agreed well with the experimental data.

NOMENCLATURE

b	air gap thickness (m)
c	concentration (mol/m^3)
C_p	specific heat (J/kg·°C)
d_h	hydraulic diameter (m)
D	diffusion coefficient (m^2/s)
EE	evaporation efficiency (—)
g	gravitational acceleration (m/s^2)
h	heat transfer coefficient (W/m^2·K)
h_d	condensate film heat transfer coefficient (W/m^2·K)

HL	heat lost (kJ/kg)
J_v	volumetric flux ($m^3/m^2 \cdot s$)
k	thermal conductivity (W/mK)
l	thickness of the cooling plate (m)
L	height of the air gap (m)
n	mass flux ($kg/m^2 \cdot s$)
N	molar flux ($mol/m^2 \cdot s$)
Nu	Nusselt number (—)
P	total pressure (N/m^2)
$P°$	vapor pressure (N/m^2)
$P*$	partial pressure (N/m^2)
Pr	Prandtl number (—)
q	heat flux (W/m^2)
q_s	sensible heat flux (W/m^2)
Q	volumetric flow rate (m^3/s)
R	gas constant ($m^3 \cdot Pa/kmol \cdot K$)
Re	Reynolds number (—)
Sc	Scmidt number (—)
Sh	Sherwood number (—)
T	temperature (K)
U	heat transfer coefficient ($W/m^2 \cdot K$)
y	mole fraction in the vapor phase (—)
z	distance (m)

Subscripts and Superscripts

a	air
av	average
b	bulk
c	cooling water
C	stagnant phase
g	gas mixture
h	hot region
I	interface
l	liquid
lm	log mean
m	membrane
p	permeate
T	temperature
w	water

Greek Letters

δ	membrane thickness (m)
β	membrane characteristic coefficient ($kg/m^2 \cdot s \cdot kPa$)

Δ difference (—)
ϵ porosity (—)
η dimensionless distance (—)
λ latent heat of vaporization (J/kg)
μ viscosity (kg/m·s)
θ dimensionless heat transfer coefficient (—)
ρ density (kg/m^3)
τ tortuosity (—)

REFERENCES

1. K. S. Spiegler, *Salt-Water Purification*, 2nd ed., Plenum Press, New York, NY, 1977.
2. F. Banat and J. Simandl, *Desalination*, *95*, 39 (1995).
3. Y. Wu, Y. Kong, X. Lin, J. Liu, J. Zhang, and J. Xu, *J. Membr. Sci.*, *72*, 189 (1992).
4. S. I. Andersson, N. Kjellander, and B. Rodesjo, *Desalination*, *61*, 237 (1987).
5. S. Kubota, K. Ohta, I. Hayaro, M. Hirai, K. Kikuchi, and M. Murayama, *Ibid.*, *69*, 19 (1988).
6. V. Calabro, B. Jiao, and E. Drioli, *Ind. Eng. Res.*, *33*, 1803 (1994).
7. Newsletter of Gordon's Cave a Vin "LA CAVE," Spring 94, Montreal, Canada.
8. S. Kimura and S. Nakao, *J. Membr. Sci.*, *33*, 285 (1987).
9. K. Sakai, T. Koyano, and T. Muroi, *Chem. Eng. J.*, *38*, B33 (1988).
10. C. Gostoli and G. C. Sarti, *J. Membr. Sci.*, *41*, 211 (1989).
11. H. Udriot, S. Ampuero, I. Marrison, and U. Stockar, *Biotechnol. Lett.*, *II*, 509 (1984).
12. E. Drioli and Y. Wu, *Desalination*, *53*, 339 (1985).
13. K. Ohta, K. Kikuchi, I. Hayano, T. Okabe, T. Goto, and S. Kimura, *Ibid.*, *78*, 177 (1990).
14. K. Ohta, I. Hayano, T. Okabe, S. Kimura, and H. Ohya, *Ibid.*, *81*, 107 (1991).
15. M. C. Porter, *Handbook of Industrial Membrane Technology*, Noyes Publishers, NJ, 1990.
16. R. C. Carson and J. Simandl, *Miner. Eng.*, *7*, 511 (1994).
17. C. Geankoplis, *Transport Processes and Unit Operations*, 3rd ed., Prentice-Hall, Englewood Cliffs, NJ, 1993.
18. A. Colburn and T. Drew, *Trans. AIChE*, *33*, 197 (1937).
19. A. H. P. Skelland, *Diffusional Mass Transfer*, Wiley, New York, NY, 1974.
20. J. P. Holman, *Heat Transfer*, McGraw-Hill, New York, NY, 1986.
21. M. Jacob, *Heat Transfer*, Wiley, New York, NY, 1958.
22. E. Matthiasson and B. Sivik, *Desalination*, *35*, 59 (1980).
23. V. Gekas and B. Hallstrom, *J. Membr. Sci.*, *30*, 153 (1987).
24. R. M. Felder and R. W. Rousseau, *Elementary Principles of Chemical Processes*, 2nd ed., Wiley, New York, NY, 1986.
25. E. Drioli, V. Calbro, and Y. Wu, *Pure Appl. Chem.*, *5*, 1657 (1986).
26. A. Bejan, *Convective Heat Transfer*, Wiley, New York, NY, 1984.
27. W. Schofield, A. G. Fane, and C. J. Fell, *Ibid.*, *53*, 173 (1990).
28. M. Findley, V. Tanna, Y. Rao, and C. Yeh, *AIChE J.*, *15*, 483–489 (1969).

Received by editor May 1, 1997